NUCL SCI TECH (2017) 28:113
DOI 10.1007/s41365-017-0267-y

The cross section calculation of ^{112}Sn(α,γ)^{116}Te reaction with different nuclear models at the astrophysical energy range

C. Yalçın[1]

Received: 16 January 2017 / Revised: 6 March 2017 / Accepted: 9 March 2017 / Published online: 5 July 2017

Abstract The theoretical cross section calculations for the astrophysical p process are needed because most of the related reactions are technically very difficult to be measured in the laboratory. Even if the reaction was measured, most of the measured reactions have been carried out at the higher energy range from the astrophysical energies. Therefore, almost all cross sections needed for p process simulation have to be theoretically calculated or extrapolated to the astrophysical energies. $^{112}\mathrm{Sn}(\alpha,\gamma)^{116}\mathrm{Te}$ is an important reaction for the p process nucleosynthesis. The theoretical cross section of $^{112}\mathrm{Sn}(\alpha,\gamma)^{116}\mathrm{Te}$ reaction was investigated for different global optical model potentials, level density, and strength function models at the astrophysically interested energies. Astrophysical S factors were calculated and compared with experimental data available in the EXFOR database. The calculation with the optical model potential of the dispersive model by Demetriou et al., and the back-shifted Fermi gas level density model and Brink-Axel Lorentzian strength function model best served to reproduce experimental results at an astrophysically relevant energy region. The reaction rates were calculated with these model parameters at the p process temperature and compared with the current version of the reaction rate library Reaclib and Starlib.

Keywords Astrophysical p process · Sn-112 · Nuclear model calculation · Talys 1.8 · Reaction rate

✉ C. Yalçın
caner.yalcin@kocaeli.edu.tr

[1] Department of Physics, Kocaeli University, 41380 Umuttepe, Kocaeli, Turkey

1 Introduction

Although there have been significant studies conducted to explain nucleosynthesis, questions still remain on production of the nuclei heavier than iron. The p process (or γ-process) is one of the astrophysical processes that is responsible for the production of proton-rich nuclei. These nuclei are located along the proton-rich side of the stability line between Se and Hg, and these nuclei are referenced as p-nuclei [1–3]. Burbidge et al. [4] and Cameron [5] suggested that p-nuclei are produced by the massive stars through photodecomposition at very high temperature in a stellar environment. The production mechanism is composed of mostly (γ, n), (γ, p), and (γ,α) reactions on preexisting s and r seed nuclei in the temperature range between 2 and 3 GK. [1, 6–8]. The astrophysically relevant energy range for the charged-particle-induced nuclear reactions is called Gamow window. The Gamow windows of astrophysical reactions were numerically calculated by Rauscher [9].

In order to simulate the p process, it is required that a large set of information be known, including nuclear parameters. This information consists of the accurate initial seed abundances, which are coming from s and r-process model calculations, the description of the stellar medium, and the nuclear properties such as reaction cross sections, reaction rates, nuclear masses, and decay rates. This information is needed directly or indirectly for the p process network simulation. In view of the nuclear parameters, the reaction rates, which are derived from cross sections of more than 20,000 reactions involving about 2000 nuclei, are needed for the p process simulation [10]. However, there are few reaction cross sections experimentally measured at the astrophysical relevant energies. The reason for

this is most of the related reactions need a radioactive target and beam, also the cross sections at the astrophysical energies are very small to measure with current technology. Because of these experimental limitations, almost all reaction cross sections (or the reaction rates) needed for the p process must be calculated theoretically.

On the other hand, measured experimental cross sections are needed to be extrapolated to the astrophysical energies because most of the experiments have been performed at higher energies than astrophysical energies [11–16]. An alternative method to the extrapolation of the experimental cross sections to lower energies is to calculate the cross sections theoretically by using the best nuclear parameters that are deduced from the comparison of the experimental results at energies close to the astrophysical energies. Then, using the best parameters, the cross sections can be calculated for the all energy ranges relevant to the p process.

The ^{112}Sn is an important p-nucleus, and the cross section measurements were experimentally performed at energies close to astrophysically relevant energies using different methods [17–20]. The Gamow window of $^{112}\mathrm{Sn}(\alpha,\gamma)^{116}\mathrm{Te}$ reaction is between $E_{\mathrm{Lab}} = 6.38$ and $E_{\mathrm{Lab}} = 10.07$ MeV at the temperature of 3 GK. ^{112}Sn also has special importance because it has a magic proton number ($Z = 50$), and it is a closed-shell nucleus. Consequently, $^{112}\mathrm{Sn}(\alpha,\gamma)^{116}\mathrm{Te}$ reaction was chosen for investigation in order to understand the effect of different nuclear models entering the cross section calculations, such as nucleon-nucleus optical model potentials (OMP), level density models (LDM), and γ-ray strength function models (SFM).

The main steps of this study are (1) investigation of the global nuclear models effects which are entering the cross section calculation, (2) comparison with the experimental data and suggesting best global parameters, and (3) calculating the reaction rate with the best model parameters of $^{112}\mathrm{Sn}(\alpha,\gamma)^{116}\mathrm{Te}$ reaction and comparing with currently used reaction rates of the Reaclib $v2.2$ [21] and Starlib $v6$ [22].

2 Model calculations and results

The nuclear model calculations were carried out using the Talys computer code (version number 1.8) [23] which is used for the analysis and prediction of nuclear reactions. It is compatible for the simulation of nuclear reactions that involve neutrons, photons, protons, deuterons, tritons, ^{3}He-, and α-particles in the 1 keV–200 MeV energy range and target nuclides of mass 12 and heavier. The cross sections of $^{112}\mathrm{Sn}(\alpha,\gamma)^{116}\mathrm{Te}$ reaction were calculated for combination of different optical model potentials (OMP), level density models (LDM), and strength function models (SFM) in order to investigate the effect of the different nuclear input parameters.

2.1 Optical model potentials

The cross sections of $^{112}\mathrm{Sn}(\alpha,\gamma)^{116}\mathrm{Te}$ reaction were calculated for eight different global alpha optical model potentials: normal alpha potential [24], McFadden and Satchler [25], Demetriou et al. [26] (in three version; Tables 1, 2, and dispersive model), Avrigeanu et al. [27], Nolte et al. [28], and Avrigeanu et al. [29]. The level density and strength function model were set to constant temperature-Fermi gas model (LDM-1) and Brink-Axel Lorentzian model (SFM-2), respectively, which are the default settings of the Talys code. The calculated cross sections with different optical model potentials were scaled to experimental cross sections of the Özkan et. al. [18], which was measured precisely and in a wide energy range among the other experiments [17, 19, 20]. The optical model potentials used in the cross section calculation are given at Table 1 (also labeled in Fig. 1). As shown in Fig. 1, the best energy dependence of the calculated cross section was the dispersive model of Demetriou et al. [26] (OMP-5). This optical potential model almost reproduces the experimental data within the experimental uncertainty except for the lowest energy point. All other optical model potentials were significantly higher than the experimental cross sections, especially at the astrophysically relevant energies.

2.2 Level density models

The optical model potential and strength function model were set to the dispersive model of Demetriou et al. (OMP-5) and the Brink-Axel Lorentzian model (SFM-2), respectively, in order to investigate the effect of different level density models on the cross section calculation of

Table 1 The different optical model potentials which are available in the Talys code. The default option is the normal alpha potential (OMP-1)

Model no	Optical model potential
OMP-1	Normal alpha potential [24]
OMP-2	McFadden and Satchler [25]
OMP-3	Demetriou et al. (Table 1) [26]
OMP-4	Demetriou et al. (Table 2) [26]
OMP-5	Demetriou et al. (dispersive model) [26]
OMP-6	Avrigeanu et al. [27]
OMP-7	Nolte et al. [28]
OMP-8	Avrigeanu et al. [29]

Table 2 Different level density model, which is available in the Talys code. The default option is constant temperature + Fermi gas model (LDM-1)

Model no	Level density model
LDM-1	Constant temperature + Fermi gas model [30]
LDM-2	Back-shifted Fermi gas model [31, 32]
LDM-3	Generalized superfluid model [33, 34]
LDM-4	Microscopic level densities (Skyrme force) [35] from Goriely's tables
LDM-5	Microscopic level densities (Skyrme force) [36] from Hilaire's combinatorial tables
LDM-6	Microscopic LD (temperature dependent HFB, Gogny force) from Hilaire's combinatorial tables (2014) [37]

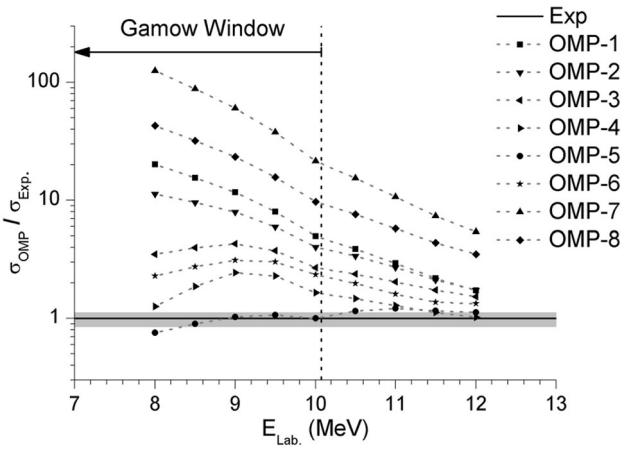

Fig. 1 The ratio of the calculated cross sections of the different optical model potential (OMP) to the experimental results of the Özkan et. al. [18]. The level density model and strength function were set the constant temperature + Fermi gas model [30] (LDM-1) and the Brink-Axel Lorentzian model [40, 41] (SFM-2), respectively. The *dotted line* connecting the points is a guide for the eye

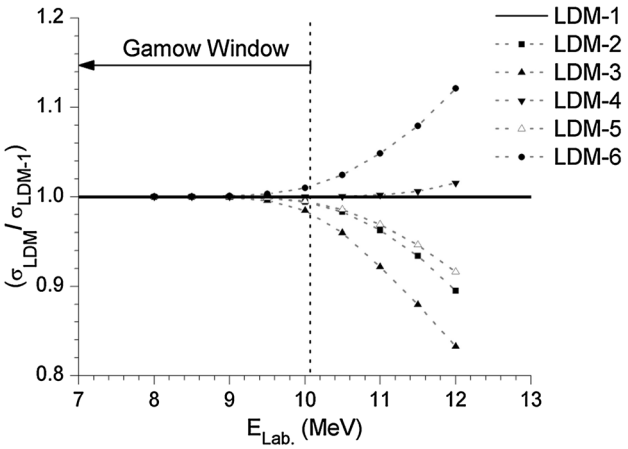

Fig. 2 The calculated cross sections ratio of the level density model of constant temperature + Fermi gas model [30] (LDM-1) to the other level density models (LDM) (see Table 2). The *dotted line* connecting the points is a guide for the eye

$^{112}Sn(\alpha,\gamma)^{116}Te$ reaction. The cross sections were then calculated with different phenomenological and microscopic level density models, which are given in Table 2. Figure 2 shows the ratio of the cross section calculation results with different level density models to that with the default level density model (LDM-1). As shown in Fig. 2, the cross section deviations are less than 2% in the Gamow window. With the increasing energy, cross section results increase for microscopic level densities of [35] and [37] (LDM-4 and LDM-6), whereas they decrease for the back-shifted Fermi gas model [31, 32], Generalized superfluid model [33, 34], and microscopic level densities of [36] (LDM-2, LDM-3, and LDM-5).

2.3 Strength function models

The cross section of $^{112}Sn(\alpha,\gamma)^{116}Te$ reaction also depends on the gamma strength function. For this reason, the contributions of eight gamma strength function models to the cross section were investigated and are given in Table 3. The optical model potential and level density model were set to the dispersive model of Demetriou et al. [26] (OMP-5) and back-shifted Fermi gas model [31, 32] (LDM-2), respectively. Figure 3 shows the ratio of the cross sections obtained from each strength function model to the cross section from Brink-Axel Lorentzian model (SFM-2). The Brink-Axel Lorentzian (SFM-2) and Gogny D1M HFB + QRPA (SFM-8) models give almost the same results at all energy points, while the other strength function models estimate lower cross section values. The highest difference in the cross section is around 15% in the Gamow Window.

3 Discussion and conclusion

Based on the results of cross section calculations with different optical model potentials, level density models, and strength function models, it is found that cross section of $^{112}Sn(\alpha,\gamma)^{116}Te$ reaction has a strong dependence on the optical model potentials. On the other hand, cross section calculations with different level density models and

Table 3 Different gamma-ray strength function model which is available in the Talys code. The default option is Brink-Axel Lorentzian model (SFM-2)

Model no	Strength function model
SFM-1	Kopecky-Uhl generalized Lorentzian [38, 39]
SFM-2	Brink-Axel Lorentzian [40, 41]
SFM-3	Hartree–Fock BCS tables [42]
SFM-4	Hartree–Fock–Bogolyubov tables [43]
SFM-5	Goriely's hybrid model [44]
SFM-6	Goriely T-dependent HFB [37]
SFM-7	T-dependent RMF [45]
SFM-8	Gogny D1M HFB+QRPA [46]

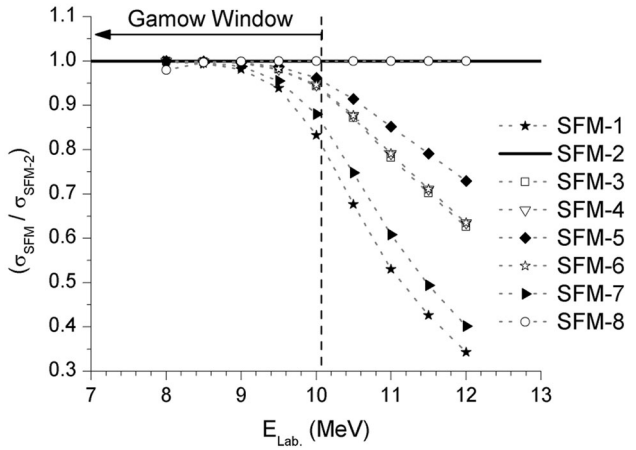

Fig. 3 The cross section ratios of different strength function models to the Brink-Axel Lorentzian model [40, 41] (see Table 3). The optical model potential and level density model were set to dispersive model of Demetriou et al. [26] (OMP-5) and back-shifted Fermi gas model [31, 32] (LDM-2), respectively. The *dotted line* connecting the points is a guide for the eye

strength function models give comparable results in the Gamow window. As a result, the cross section calculation with the combination of dispersive model of Demetriou et al. [26] (OMP-5), back-shifted Fermi gas level density model (LDM-2), and the Brink-Axel Lorentzian strength function model (SFM-2) best reproduced the experimental cross sections.

Because the charged-particle cross section is highly energy dependent, extrapolation of the cross section to the lower energies and the comparison between theoretical and experimental results in the low energy region are very difficult. The astrophysical S factor removes the part of the strong energy dependence of the cross section by accounting for the s-wave Coulomb barrier transmission, $\exp(-2\pi\eta)$, at low energies. For this reason, it is a useful tool for the analysis of charged-particle reactions. The S factor is defined as [47]

$$S(E) = \sigma(E)E\mathrm{e}^{2\pi\eta}, \tag{1}$$

where η is the Sommerfeld parameter, as defined in reference [47]. The astrophysical S factors were calculated from the cross sections with the best model combination (OMP-5, LDM-2, SFM-2) and compared with experimental results. The experimental results of Özkan et. al. [18] were well described by the theoretical calculation with this model combination (see Fig. 4).

The reaction rates, which are needed for the p process simulation, were also calculated using the best model combination (OMP-5, LDM-2, SFM-2). The average reaction rate per particle pair at a given stellar temperature T^* is defined by:

$$\langle\sigma v\rangle^* = \left(\frac{8}{\pi\mu}\right)^{1/2}\frac{1}{(kT^*)^{3/2}} \int_0^\infty \sigma^*_{(\alpha,\gamma)}(E)E\exp\left(-\frac{E}{kT^*}\right)\mathrm{d}E, \tag{2}$$

by folding the stellar reaction cross section $\sigma^*_{(\alpha,\gamma)}(E)$ with the Maxwell–Boltzmann velocity distribution of the nuclei [47]. Here, μ is the reduced mass of the system. The nuclei can also be found in excited states in the stellar plasma; therefore, the stellar reaction cross section $\sigma^* = \sum_\lambda \sigma^\lambda$ includes transitions from all populated target states λ to all energetically possible final states, ν, whereas a laboratory cross section $\sigma^{\mathrm{lab}} = \sum_\nu \sigma^{0\nu}$ only accounts for transitions from the ground states of the target. The ratio of the stellar to laboratory reaction cross section, $\sigma^*/\sigma^{\mathrm{lab}}$, is called the stellar enhancement factor. Since there is no low-lying excited state in ^{112}Sn, stellar enhancement factor of $^{112}\mathrm{Sn}(\alpha,\gamma)^{116}\mathrm{Te}$ reaction is negligible at the p process temperature of $2.0 \le T_9 \le 3.0$ (where T_9 is the temperature in GK).

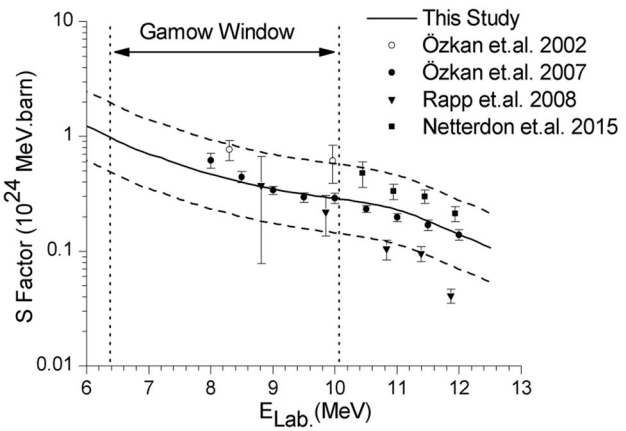

Fig. 4 Theoretically and experimentally calculated astrophysical S factors. The Gamow window is also shown in the figure for the temperature of 3 GK. *Dashed lines* are showing the calculated S factors multiplied by 0.5 and 2

Reaction rate results are given in Table 4. Figure 5 shows the comparison of the calculated reaction rates with those in the Reaclib *v*2.2 (data set; ths8(v4)) [21] and Starlib *v*6 [22]. It is found that calculated reaction rates are in excellent agreement with those reported by Starlib *v*6 [22], while they are considerably lower than those reported by Reaclib *v*2.2 [21].

The theoretical calculations of the cross sections are as important as the experimental efforts to study the nucleosynthesis theory. In this study, the cross sections of $^{112}Sn(\alpha,\gamma)^{116}Te$ reaction were calculated with different optical model potentials, level density models, and strength function models in order to understand the effect of different nuclear parameters. The conclusions of this study can be summarized as follows:

- The cross section calculations are very sensitive to global optical model potentials (OMP) for $^{112}Sn(\alpha,\gamma)^{116}Te$ reaction. The sensitivity to optical model potentials is increasing with decreasing energy.
- The different level density models contribution to cross section calculations is very limited in the Gamow windows.
- The cross section difference for different strength function models is less than 15% in the Gamow window.

Table 4 The calculated reaction rates with the best model parameters (OMP-5, LDM-2, SFM-2)

Temperature (GK)	Reaction rate $cm^3/mol\,s$
0.25	3.27E−65
0.3	2.55E−59
0.4	1.58E−50
0.5	2.44E−44
0.6	1.88E−39
0.7	1.48E−35
0.8	1.98E−32
0.9	7.00E−30
1	9.32E−28
1.5	1.31E−20
2	4.13E−16
2.5	7.55E−13
3	2.42E−10
3.5	2.31E−8
4	8.22E−7
5	9.19E−5
6	0.00154
7	0.0113
8	0.0504
9	0.158
10	0.374

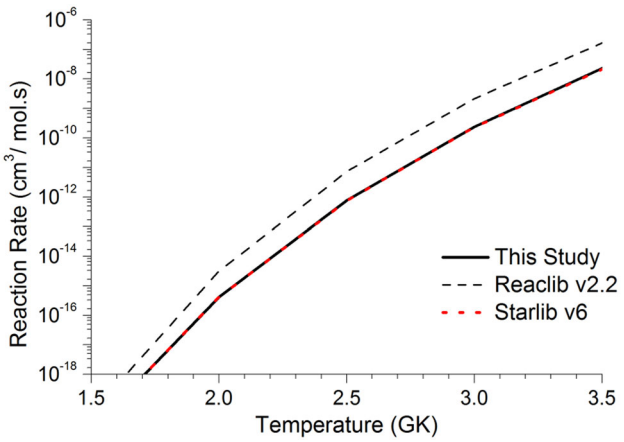

Fig. 5 (Color online) The comparison of the calculated reaction rates with the Reaclib *v*2.2 [21] and Starlib *v*6 [22] rate libraries for $^{112}Sn(\alpha,\gamma)^{116}Te$ reaction. The reaction rates are shown for the p process temperatures, for all temperature scale see Table 4

- The optical model potential of the dispersive model by Demetriou et al. with the combination of the back-shifted Fermi gas level density model and the Brink-Axel Lorentzian strength function model best reproduces the experimental *S* factor (or cross section) results by Özkan et. al. [18].
- The calculated *S* factors agree with all of the experimental results within a factor of 2, except the highest energy point by Rapp et al. [19].
- The reaction rate library by Reaclib *v*2.2 [21] overestimated the reaction rates. The calculated reaction rate results are 7–10 times lower than those by Reaclib *v*2.2 in the *p* process temperature of 2–3 GK.
- The calculated reaction rates are in excellent agreement with Starlib *v*6 [22] in the temperature range of 1–3.5 GK.

As a result, new reaction rate values (see Table 4) for $^{112}Sn(\alpha,\gamma)^{116}Te$ reaction are suggested to the *p* process nucleosynthesis simulation. The investigation of other nuclear reactions related to *p* process nucleosynthesis will help to develop a reliable nucleosynthesis theory.

References

1. S.E. Woosley, W.M. Howard, The p-process in supernovae. Astrophys. J. Suppl. Ser. **36**, 285–304 (1978). doi:10.1086/190501
2. M. Arnould, S. Goriely, The p-process of stellar nucleosynthesis: astrophysics and nuclear physics status. Phys. Rep. **384**, 1–84 (2003). doi:10.1016/S0370-1573(03)00242-4
3. T. Rauscher, N. Dauphas, I. Dillmann et al., Constraining the astrophysical origin of the p-nuclei through nuclear physics and meteoritic data. Rep. Prog. Phys. **76**, 066201 (2013). doi:10.1088/0034-4885/76/6/066201

4. E.M. Burbidge, G.R. Burbidge, W.A. Fowler et al., Synthesis of the elements in stars. Rev. Mod. Phys. **29**, 547 (1957). doi:10.1103/RevModPhys.29.547
5. A.G.W. Cameron, Chalk River, Stellar Evolution, Nuclear Astrophysics, and Nucleogenesis (CRL-41). Rep. CRL, Vol. 41 (Atomic Energy of Cande Ltd., 1957)
6. W. Rapp, J. Görres, M. Wiescher et al., Sensitivity of p-process nucleosynthesis to nuclear reaction rates in a $25M_{\odot}$ supernova model. Astrophys. J. **653**, 474 (2006)
7. T. Rauscher, Branchings in γ process path revisited. Phys. Rev. C **73**, 015804 (2006). doi:10.1103/PhysRevC.73.015804
8. P. Mohr, Zs Fülöp, H. Utsunomiya, Photo-induced nucleosynthesis. Phys. J. A **32**, 357–369 (2007). doi:10.1140/epja/i2006-10378-y
9. T. Rauscher, Relevant energy ranges for astrophysical reaction rates. Phys. Rev. C **81**, 045807 (2010). doi:10.1103/PhysRevC.81.045807
10. T. Sauter, F. Kappeler, (p, γ) rates of ^{92}Mo, ^{94}Mo, ^{95}Mo, ^{98}Mo: towards an experimentally founded database for p-process studies. Phys. Rev. C **55**, 3127 (1997). doi:10.1103/PhysRevC.55.3127
11. Gy. Gyürky, Z. Elekes, J. Farkas et al., Alpha-induced reaction cross section measurements on ^{151}Eu for the astrophysical gamma-process. J. Phys. G: Nuclear Part. Phys. **37**, 115201 (2010). doi:10.1088/0954-3899/37/11/115201
12. P. Scholz, A. Endres, A. Hennig et al., Measurement of the $^{187}\mathrm{Re}(\alpha,\mathrm{n})^{190}Ir$ reaction cross section at sub-Coulomb energies using the Cologne Clover counting setup. Phys. Rev. C **90**, 065807 (2014). doi:10.1103/PhysRevC.90.065807
13. C. Yalçın, Gy. Gyürky, T. Rauscher et al., Test of statistical model cross section calculations for α induced reactions on ^{107}Ag at energies of astrophysical interest. Phys. Rev. C **91**, 034610 (2015). doi:10.1103/PhysRevC.91.034610
14. R.T. Güray, N. Özkan, C. Yalçın et al., Measurements of $^{152}\mathrm{Gd}(\mathrm{p},\gamma)^{153}$Tb and $^{152}\mathrm{Gd}(\mathrm{p,n})^{152}$Tb reaction cross sections for the astrophysical γ process. Phys. Rev. C **91**, 055809 (2015). doi:10.1103/PhysRevC.91.055809
15. Z. Halasz, E. Somorjai, Gy. Gyürky et al., Experimental study of the astrophysical gamma-process reaction $^{124}\mathrm{Xe}(\alpha,\gamma)^{128}$Ba. Phys. Rev. C **94**, 045801 (2016). doi:10.1103/PhysRevC.94.045801
16. J. Mayer, S. Goriely, L. Netterdon et al., Partial cross sections of the $^{92}\mathrm{Mo}(\mathrm{p},\gamma)$ reaction and the gamma strength in ^{93}Tc. Phys. Rev. C **93**, 045809 (2016). doi:10.1103/PhysRevC.93.045809
17. N. Özkan, A.St.J. Murphy, R.N. Boyd et al., Cross section measurements of the $^{102}\mathrm{Pd}(\mathrm{p},\gamma)^{103}$Ag, $^{116}\mathrm{Sn}(\mathrm{p},\gamma)^{117}$Sb, and $^{112}\mathrm{Sn}(\alpha,\gamma)^{116}$Te reactions relevant to the astrophysical rp- and γ-processes. Nucl. Phys. A **710**, 469–485 (2002). doi:10.1016/S0375-9474(02)01134-X
18. N. Özkan, G. Efe, R.T. Güray et al., Astrophysical S factor for α-capture on ^{112}Sn in the p-process energy range. Phys. Rev. C **75**, 025801 (2007). doi:10.1103/PhysRevC.75.025801
19. W. Rapp, I. Dillmann, F. Käppeler et al., Cross section measurements of α-induced reactions on ^{92,94}Mo and ^{112}Sn for p-process studies. Phys. Rev. C **78**, 025804 (2008). doi:10.1103/PhysRevC.78.025804
20. L. Netterdon, J. Mayer, P. Scholz et al., Total and partial cross sections of the $^{112}\mathrm{Sn}(\alpha,\gamma)^{116}$Te reaction measured via in-beam γ-ray spectroscopy. Phys. Rev. C **91**, 035801 (2015). doi:10.1103/PhysRevC.91.035801
21. R.H. Cyburt, A.M. Amthor, R. Ferguson et al., The JINA reaclib database: its recent updates and impact on type-I X-ray bursts. Astrophys. J. Suppl. Ser. **189**, 240–252 (2010). doi:10.1088/0067-0049/189/1/240
22. A.L. Sallaska, C. Iliadis, A.E. Champange et al., Starlib: a next-generation reaction-rate library for nuclear astrophysics. Astrophys. J. Suppl. Ser. **207**, 18 (2013). doi:10.1088/0067-0049/207/1/18
23. A.J. Koning, S. Hilaire, M.C. Duijvestijn, TALYS-1.0, in Proceedings of the International Conference on Nuclear Data for Science and Technology, April 22–27, 2007, Nice, France, ed. by O. Bersillon, F. Gunsing, E. Bauge, R. Jacqmin, and S. Leray, EDP Sciences, pp. 211–214 (2008)
24. S. Watanabe, High energy scattering of deuterons by complex nuclei. Nucl. Phys. **8**, 484–492 (1958). doi:10.1016/0029-5582(58)90180-9
25. L. McFadden, G.R. Satchler, Optical-model analysis of the scattering of 24.7 MeV alpha particles. Nucl. Phys. **84**, 177–200 (1966). doi:10.1016/0029-5582(66)90441-X
26. P. Demetriou, C. Grama, S. Goriely, Improved global α-optical model potentials at low energies. Nucl. Phys. A **707**, 253–276 (2002). doi:10.1016/S0375-9474(02)00756-X
27. V. Avrigeanu, M. Avrigeanu, C. Manailescu, Further explorations of the α-particle optical model potential at low energies for the mass range $A \approx 45$–209. Phys. Rev. C **90**, 044612 (2014). doi:10.1103/PhysRevC.90.044612
28. M. Nolte, H. Machner, J. Bojowald, Global optical potential for α particles with energies above 80 MeV. Phys. Rev. C **36**, 1312 (1987). doi:10.1103/PhysRevC.36.1312
29. V. Avrigeanu, P.E. Hodgson, M. Avrigeanu, Global optical potentials for emitted alpha particles. Phys. Rev. C **49**, 2136 (1994). doi:10.1103/PhysRevC.49.2136
30. A. Gilbert, A.G.W. Cameron, A composite nuclear-level density formula with shell corrections. Can. J. Phys. **43**, 1446–1496 (1965). doi:10.1139/p65-139
31. W. Dilg, W. Schantl, H. Vonach et al., Level density parameters for the back-shifted fermi gas model in the mass range $40 < A < 250$. Nuclear Phys. A **217**, 269–298 (1973). doi:10.1016/0375-9474(73)90196-6
32. P. Demetriou, S. Goriely, Microscopic nuclear level densities for practical applications. Nuclear Phys. A **695**, 95–108 (2001). doi:10.1016/S0375-9474(01)01095-8
33. A.V. Ignatyuk, K.K. Istekov, G.N. Smirenkin, The role of collective effects in the systematics of nuclear level densities. Sov. J. Nuclear Phys. **29**(4), 450 (1979)
34. A.V. Ignatyuk, J.L. Weil, S. Raman et al., Density of discrete levels in ^{116}Sn. Phys. Rev. C **47**, 1504 (1993). doi:10.1103/PhysRevC.47.1504
35. S. Goriely, S. Hilaire, A.J. Koning, Improved microscopic nuclear level densities within the Hartree-Fock-Bogoliubov plus combinatorial method. Phys. Rev. C **78**, 064307 (2008). doi:10.1103/PhysRevC.78.064307
36. S. Hilaire, S. Goriely, Global microscopic nuclear level densities within the HFB plus combinatorial method for practical applications. Nucl. Phys. A **779**, 63 (2006). doi:10.1016/j.nuclphysa.2006.08.014
37. S. Hilaire, M. Girod, S. Goriely et al., Temperature-dependent combinatorial level densities with the D1M Gogny force. Phys. Rev. C **86**, 064317 (2012). doi:10.1103/PhysRevC.86.064317
38. J. Kopecky, M. Uhl, R.E. Chrien, Radiative strength in the compound nucleus ^{157}Gd. Phys. Rev. C **47**, 312 (1993). doi:10.1103/PhysRevC.47.312
39. J. Kopecky, M. Uhl, Test of gamma-ray strength functions in nuclear reaction model calculations. Phys. Rev. C **41**, 1941 (1990). doi:10.1103/PhysRevC.41.1941
40. D.M. Brink, Individual particle and collective aspects of the nuclear photoeffect. Nuclear Phys. **4**, 215–220 (1957). doi:10.1016/0029-5582(87)90021-6
41. P. Axel, Electric dipole ground-state transition width strength function and 7 Mev photon interactions. Phys. Rev. **126**, 671 (1962). doi:10.1103/PhysRev.126.671

42. S. Goriely, E. Khan, Large-scale QRPA calculation of E1-strength and its impact on the neutron capture cross section. Nuclear Phys. A **706**, 217–232 (2002). doi:10.1016/S0375-9474(02)00860-6
43. S. Goriely, E. Khan, M. Samyn, Microscopic HFB + QRPA predictions of dipole strength for astrophysics applications. Nuclear. Phys. A **739**, 331–352 (2004). doi:10.1016/j.nuclphysa.2004.04.105
44. S. Goriely, Radiative neutron captures by neutron-rich nuclei and the r-process nucleosynthesis. Phys. Lett. B **436**, 10–18 (1998). doi:10.1016/S0370-2693(98)00907-1
45. D.P. Arteaga, P. Ring, Relativistic random-phase approximation in axial symmetry. Phys. Rev. C **77**, 034317 (2008). doi:10.1103/PhysRevC.77.034317
46. M. Martini, S. Hilaire, S. Goriely et al., Improved nuclear inputs for nuclear model codes based on the gogny interaction. Nuclear Data Sheets **118**, 273–275 (2014). doi:10.1016/j.nds.2014.04.056
47. C.E. Rolfs, W.S. Rodney, *Cauldrons in the Cosmos* (The University of Chicago Press, Chicago, 1988)